

# Demonstration of a Silicon Ring Resonator Coupling-Modulator-based Coherent Optical Sub-Assembly Operating at 802 Gbps

X. Chen<sup>(1),†</sup>, A. Mistry<sup>(2),†</sup>, M. Bahadori<sup>(2)</sup>, K. Padmaraju<sup>(2)</sup>, M. Malinowski<sup>(2)</sup>, D. Che<sup>(1)</sup>, R. Sukkar<sup>(2)</sup>, R. Younce<sup>(2)</sup>, A. Horth<sup>(2)</sup>, Y. Dziashko<sup>(2)</sup>, H. Guan<sup>(2)</sup>, R. Shi<sup>(2)</sup>, D. Gill<sup>(2)</sup>, A. Seyoum<sup>(2)</sup>, J. Naik<sup>(2)</sup>, D. Lim<sup>(2)</sup>, A. El Sayed<sup>(2)</sup>, A. Rylyakov<sup>(2)</sup>, M. Schmidt<sup>(2)</sup>, Z. Luo<sup>(2)</sup>, P. Magill<sup>(2)</sup>, G. Burrell<sup>(2)</sup>, J. Basak<sup>(2)</sup>, D. Chapman<sup>(2)</sup>, A. Mikami<sup>(2)</sup>, Y. Man<sup>(2)</sup>, A. Leven<sup>(2)</sup>, N. A. F. Jaeger<sup>(3)</sup>

<sup>(1)</sup> Nokia Bell Labs, New Providence, NJ, USA

<sup>(2)</sup> Nokia of America Corporation, New York, NY 10016, USA

<sup>(3)</sup> Dept. of Electrical and Computer Engineering, Univ. of British Columbia, Vancouver, Canada

† Both authors contributed equally

[xi.v.chen@nokia-bell-labs.com](mailto:xi.v.chen@nokia-bell-labs.com)

**Abstract** We present the first demonstration of a silicon ring resonator, coupling-modulation-based, dual-polarization I/Q modulator in an optical sub-assembly with integrated SiGe drivers. We demonstrate 78-km 802.6 Gbps transmission with 90-GBaud PS-64-QAM modulation. ©2023 The Author(s)

## Introduction

The relatively large discrepancy between the annual traffic growth rate (40% ~ 60%) and the data rate growth rate per coherent module (~20%) will likely push future optical transceivers towards higher levels of integration and parallelization [1]. Among the many readily available materials/platforms capable of integrating multiple transceivers into single modules, silicon photonics (SiPh) is one of the promising choices due to its stable performance, high yields, and small device footprints [2]. In these systems, minimizing the size of the components is critical to maintain a small form-factor. However, modulators still consume the largest-footprints in SiPh-based, and other material platform-based, coherent optical sub-assemblies (COSAs). While typical SiPh traveling-wave Mach-Zehnder (TWMZ) modulators have lengths of 4-7 mm, further shrinking the size/length of the modulator will result in devices with higher  $V_{\pi}$  values. The devices are not suitable or scalable for high symbol rate operation due to the limitations of high-speed electrical generation and power consumption considerations. To continue leveraging the benefits of SiPh-based platforms, the modulator architectures thus need to be modified to accommodate smaller footprints, while maintaining similar (or reducing)  $V_{\pi}$  values. Common approaches include conventional ring resonators, ring-assisted Mach Zehnder modulators, Fabry-Perot modulators, and coupling-modulated ring resonators [3]. Coupling-modulated ring resonators exhibit the same advantageous properties of TWMZs used in SiPh-based COSAs; low chirp, linear transfer functions, and binary phase transitions as the applied RF voltage passes through the null

transmission point, all while occupying much smaller footprints [4]. Due to the resonant nature of the device, the modulator  $V_{\pi}$  can be several factors smaller than the  $V_{\pi}$  of a stand-alone TWMZ, while still maintaining the bandwidth of the TWMZ itself.

In this paper, we present the first demonstration of a dual-polarization (DP) I/Q modulator based on coupling-modulated ring resonators. We flip-chip the photonic IC (PIC) onto a BGA-based COSA with co-packaged RF drivers and demonstrate 90-GBaud DP probabilistically shaped (PS)-64-QAM transmission, supporting a net data rate of 838.6 Gbps at back-to-back (B2B) and 802.6 Gbps with 78-km standard single mode fiber (SSMF) transmission.

## The coupling-modulator and the integrated coherent transmitter

A schematic of the modulator is shown in Fig. 1a. The TWMZ embedded in the drop-port of the cavity, modulates the drop-port coupling coefficient, and hence modulates the output power and phase. The embedded TWMZ gates the intracavity optical field as it exits the cavity. Because the intracavity parameters remain fixed, the modulator is not limited by the photon lifetime of the cavity, but rather by the electro-optic (EO) bandwidth of the TWMZ itself [4, 5]. The transfer function of the drop-port of a coupling-modulator is similar to that of a conventional Mach-Zehnder interferometer (MZI), as shown in Fig. 1b. Due to the high quality factor (Q-factor) of the optical cavity, small changes in the drop-port coupling allow for large swings in the optical power coupled out of the cavity, while the rest of the power is recirculated. As a result, full transmission swings can be

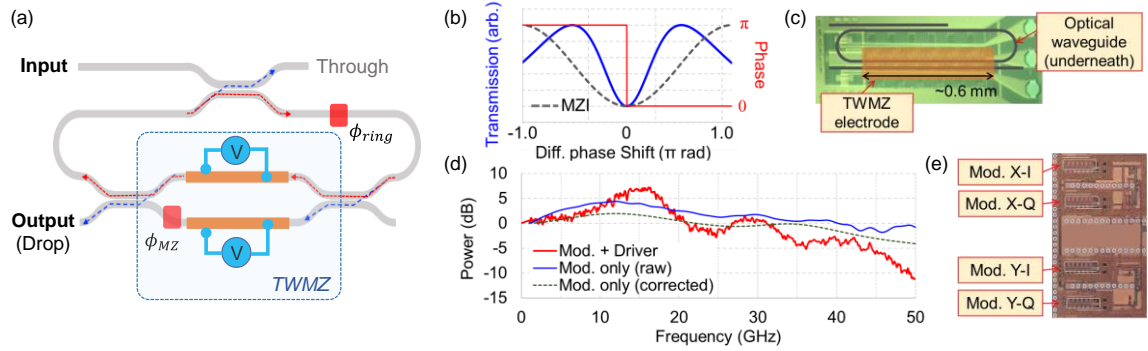


**Fig. 1:** (a) Schematic diagram of the coupling-modulator. (b) Simulated transfer functions of a coupling-modulator and a conventional MZI. (c) A microscope image of a fabricated coupling-modulator. (d) Measured EO response of one of the four modulators and the combined S21 with the driver. (e) A microscope image of the PIC.

achieved for an applied differential phase shift less than  $\pi$  radians. This effectively reduces the modulator  $V_\pi$  as compared to conventional TWMZ modulators with the same electrode length, which require a  $\pi$  radian phase shift to achieve full transmission swings. In a practical case, the  $V_\pi$  reduction is proportional to the Q-factor of the ring. In our fabricated device, with a Q-factor of  $\sim 78k$ , we have a reduction of  $\sim 50\%$ . The  $V_\pi$  of our coupling-modulator is  $\sim 14$  V. We acknowledge that this is a high  $V_\pi$ . However, a TWMZ with the same size/length would have a  $V_\pi$  of  $\sim 28$  V. The  $V_\pi$  can be further reduced by improving the resonator Q-factor and improved electrode design. Fig. 1c shows a microscope image of a single fabricated coupling-modulator on a bare die. The electrode length is  $\sim 0.6$ -mm. Including the ring structure, the modulator occupies an area of less than  $1 \text{ mm} \times 0.3 \text{ mm}$ , which can be further reduced by more compact layout. The small-signal EO response of a stand-alone coupling-modulator test structure, measured at wafer level, is shown in blue in Fig. 1d. The measurement was taken with the TWMZ slightly detuned from the null-bias condition, and with the cavity assumed to be detuned from resonance, as we did not implement a resonance-locking routine for wafer-level testing. A correction is applied to the result and the true EO response of the modulator is then plotted (in green). The 3-dB bandwidth of the modulator is  $\sim 45$  GHz. The bandwidth was limited by an impedance and delay mismatch in the transmission line. A wider bandwidth can be achieved with impedance and delay corrections. Four coupling-modulators were arranged into a DP IQ modulator configuration on a single silicon PIC. The PIC was flip-chip packaged onto an organic substrate with co-designed high-speed SiGe RF drivers. SSMFs were attached to the edge of the PIC on the BGA-based COSA for optical I/O. A microscope image of the PIC is shown in Fig. 1e. The combined bandwidth

measurement for the driver and the modulator (measured via an optical spectrum analyzer) is shown in red in Fig. 1d. The combined bandwidth is  $\sim 35$  GHz. The differences between the EO responses of four modulators were negligible. Each one of the four modulators requires two bias controls: one for the TWMZ ( $\phi_{MZ}$ ) and one for the ring ( $\phi_{ring}$ ). Thus, for a DP I/Q modulator, there are 10 bias controls (compared to 6 for conventional TWMZs). We developed a dedicated automatic bias control (ABC) algorithm for the module to maintain each modulator's bias conditions and resonance-locking to the input CW laser wavelength. All data modulation measurements were done with the ABC in-operation, without manual bias control or active temperature control of the setup.

### Experimental setup

Our experimental setup is shown in Fig. 2. The optical transmitter consists of an external cavity laser (ECL), the COSA, and a four-channel 45-GHz arbitrary waveform generator (AWG) (Keysight M8199A) operating at 128 GSa/s. The laser has a linewidth of  $< 100$  kHz and operates at  $\sim 1550$  nm. The AWG output peak-to-peak voltage is set to 500 mV (1 V per pair of differential outputs). We boost the CW power from the laser to 21.4 dBm via an EDFA. The modulator output power is -19.3 dBm. The low output power is a combined result of unexpectedly high losses from experimental edge couplers, as well as the relatively high  $V_\pi$ . The modulated light is then amplified by another EDFA before fiber transmission. The resulting transmitter side OSNR is 34.1 dB. The transmission fiber consists of a single span of 78-km SSMF. The fiber has a loss of 0.2 dB/km and a dispersion of 17 ps/km/nm. The signal is received by a standard discrete components-based coherent receiver, consisting of a free-running ECL ( $\sim 1550$  nm,  $\sim 600$  MHz away from the transmitter laser), an optical hybrid, four 75-GHz balanced photodetectors (BPD), and a real-time scope

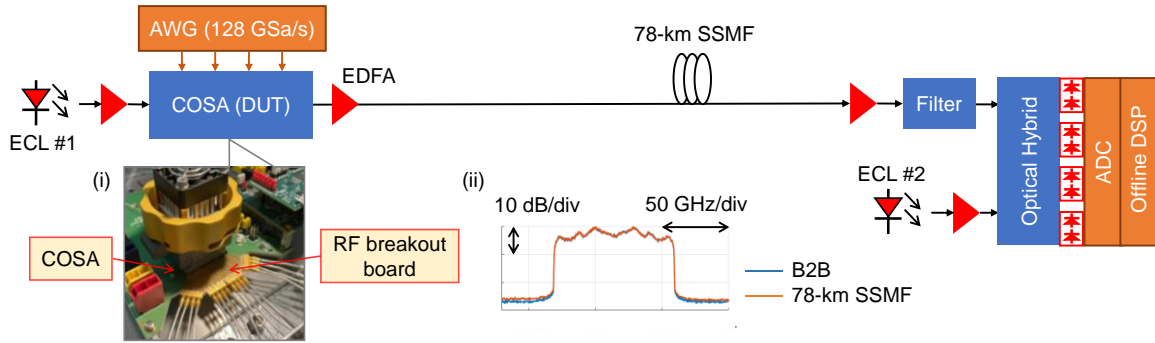


**Fig. 2:** (a) Experimental setup for the 802.6 Gbps 78-km SSMF transmission with the COSA. Inset (i) shows the COSA mounted on an evaluation board. Inset (ii) shows the measured optical spectra before and after the 78-km fiber transmission.

(256-GSa/s with 84-GHz analog bandwidth) with an offline digital signal processor (DSP).

We generate a 90-GBaud single carrier signal using root-raised-cosine (RRC) filters with a 1% spectral roll-off. We use a PS-64-QAM format and adjust the entropy of the symbols to find the highest data rate that yields a normalized generalized mutual information (NGMI) value higher than the threshold required for error-free decoding [6]. There are  $\sim 217$  random symbols used to form each of the transmitter patterns. We use a rate-0.7932 (26.07% overhead) concatenated forward error correction (FEC) coding scheme which consists of a spatially-coupled low-density parity-check (SC-LDPC) rate-0.8 inner code and a hard-decision Bose-Chaudhuri-Hocquenghem (BCH) rate-0.9915 outer code to remove potential error floors [7]. The required NGMI value for the FEC is 0.845. At the receiver, the DSP performs frequency offset compensation, dispersion compensation, frame synchronization, equalization of the waveform via a real-valued  $4 \times 4$  least mean square (LMS) equalizer operating at  $2 \times$  oversampling (2SPS), 3rd order Volterra equalization ([16, 16, 16 taps] @2SPS), and symbol decision. The LMS filter has 161 taps (894 ps).  $\sim 8,000$  symbols are used for pre-convergence, followed by blind equalization. Only the blindly recovered data is used for NGMI calculation. Roughly 2 million bits are used for the NGMI and bit error ratio (BER) calculation.

## Results and discussion

The measurement results of the 90-GBaud PS-64-QAM signals are shown in Fig. 3a. For the B2B measurement, the maximum entropy is 5.9 bits/sym/pol (constellation shaping factor  $\beta = 1.95$ ). The measured constellation signal-to-noise ratio (SNR) is 15.4 dB. The NGMI is 0.8481 and the BER is  $3.9 \times 10^{-2}$ . Using the probabilistic amplitude shaping structure [8], we have  $\gamma = 0.3796$  for PS-64-QAM. The corresponding line rate is therefore 1.06 Tbps ( $2(1+\beta) \cdot 2\text{pol} \cdot 90$  GBaud) and the net data rate is 838.6 Gbps ( $2(\gamma+\beta) \cdot 2\text{pol} \cdot 90$  GBaud). After the 78-km transmission, the SNR decreases to 15.1

dB, which allows 5.7 bits/sym/pol ( $\beta = 1.85$ ). The measured NGMI is 0.8604 and the BER is  $3.6 \times 10^{-2}$ . The net rate after the transmission is 802.6 Gbps. The insets in Fig. 3a show examples of the recovered PS-64-QAM constellations for B2B (838.6 Gbps) and after 78-km SSMF (802.6 Gbps).

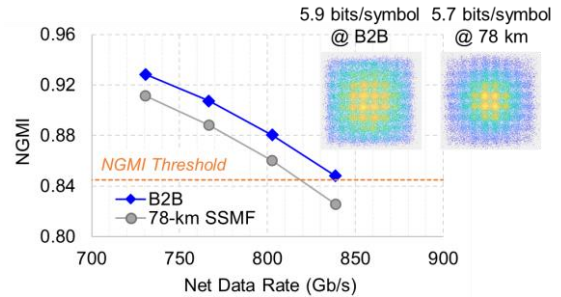


**Fig. 3** NGMI as a function of the net data rate for the 90-GBaud signal for B2B and after 78-km SSMF (at 1550nm). The insets show two recovered constellations at B2B and after 78 km fiber transmission.

We also measure 802.6 Gbps B2B transmission at several wavelengths across the C-band. As shown in Fig. 3b, the measured NGMI as a function of wavelength, for our DP I/Q coupling modulator, is very small.

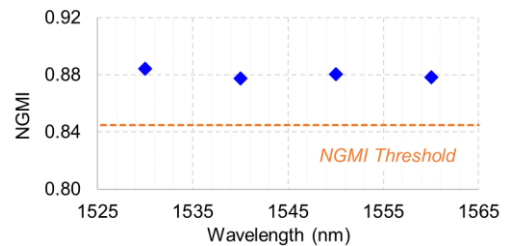


**Fig. 4** NGMIs measured for 802.6 Gbps data rate (B2B) at different wavelengths.

## Conclusion

We present the first demonstration of a SiPh DP I/Q modulator based on ring resonator coupling-modulators. The modulator is integrated with SiGe drivers in a COSA. The COSA supports 90-GBaud PS-64-QAM modulation and achieves 832.6 Gbps at B2B and 802.6 Gbps with 78-km SSMF transmission.

## References

- [1] P. J. Winzer, et al., "Fiber-optic transmission and networking: the previous 20 and the next 20 years," *Opt. Express* **26**, 24190-24239 (2018).
- [2] A. Rahim, et al. "Taking silicon photonics modulators to a higher performance level: state-of-the-art and a review of new technologies," *Adv. Photon.*, **3**(2), 024003 (2021).
- [3] W. D. Sacher, et al., "Coupling modulation of microrings at rates beyond the linewidth limit," *Opt. Express* **21**, 9722-9733 (2013).
- [4] W. D. Sacher, et al., "Binary phase-shift keying by coupling modulation of microrings," *Opt. Express* **22**, 20252-20259 (2014).
- [5] A. Mistry, et al., "FSR-free microring-based coupling modulator with integrated contra-directional-couplers," *Proc. SPIE* 11276 (2020).
- [6] J. Cho, et al., "NGMI as a Forward Error Correction Threshold for Probabilistically Shaped QAM," *ECOC 2017*, 1-3 (2017).
- [7] J. Cho, et al., "Construction of protographs for large-girth structured LDPC convolutional codes," *IEEE ICC*, 4412-4417 (2015).
- [8] G. Böcherer, et al., "Bandwidth efficient and rate-matched low-density parity-check coded modulation," *IEEE Trans. Comm.* **63**(12), 4651-4665 (2015).